Applied Catalysis A: General 450 (2013) 120–130

Contents lists available at SciVerse ScienceDirect

Applied Catalysis A: General

journal homepage: www.elsevier.com/locate/apcata

$VO_x/c\text{-}Al_2O_3$ catalyst for oxidative dehydrogenation of ethane to ethylene: Desorption kinetics and catalytic activity

S. Al-Ghamdi[a,b], M. Volpe[d], M.M. Hossain[c], H. de Lasa[a,*]

[a] Chemical Reactor Engineering Centre, Western University, London, Ontario, Canada
[b] Research & Development Center, Saudi Aramco Oil Company, Dhahran, Saudi Arabia
[c] Department of Chemical Engineering, King Fahd University of Petroleum & Minerals, Dhahran, Saudi Arabia
[d] Chemical Engineering Department, PLAPIQUI-(UNS-CONICET), Bahia Blanca, Argentina

ARTICLE INFO

Article history:
Received 9 July 2012
Received in revised form
27 September 2012
Accepted 6 October 2012
Available online 8 November 2012

Keywords:
NH_3-TPD kinetics
Oxidative dehydrogenation
Ethylene
Vanadium oxide
Lattice oxygen
Riser simulator

ABSTRACT

This study reports ethane oxidative dehydrogenation (ODH) using lattice oxygen. Ethane ODH is studied under an oxygen-free atmosphere employing a 10 wt.% VO_x supported on c-Al_2O_3. TPR and TPO show that the prepared 10 wt.% VO_x supported on c-alumina catalyst is a stable catalyst over repeated reduction and oxidation cycles. XRD shows the absence of V_2O_5 bulk surface species and a high dispersion of VO_x on the support surface. Experiments are carried out in the CREC Fluidized Bed Riser Simulator at 550–600 °C and pressures close to atmospheric conditions. Reactivity tests show that the prepared ODH catalyst displays 6.5–27.6% ethane conversion and 57.6–84.5% ethylene selectivity in the 550–600 °C range. Metal–support interaction is assessed using ammonia TPD. This provides the desorption energy for both the bare c-Al_2O_3 support and for the VO_x/c-Al_2O_3 catalyst. A slightly increased desorption energy is found when using the V-loaded catalyst. This shows low metal–support interactions and as a result, a well dispersed VO_x catalyst phase with high availability of lattice oxygen for ODH. These findings are confirmed with XRD, showing no changes with respect to the XRD for the c-Al_2O_3 alumina support. This proves that there are no other species formed due to the interaction between the VO_x surface species and the Al_2O_3 support.

© 2012 Elsevier B.V. All rights reserved.

1. Introduction

Light olefins, specifically ethylene and propylene, represent the most important building blocks of the petrochemical industry. Steam cracking of hydrocarbon feedstock (ethane, LPG, or naphtha) has been the major source of light olefins accounting for 70% of total olefin production [1]. Other methods for olefin production such as fluidized catalytic cracking (FCC) and direct dehydrogenation are also in use. Fluidized catalytic cracking (FCC) is the second most frequently used process for olefin production accounting for 28% of total gasoline production, with ethylene and propylene being in yields of 1–2% and 5%, respectively.

Current conventional processes for olefin production suffer from several limitations related to their high energy requirements due to the endothermic nature of the reaction, coke formation, selectivity control and thermodynamic constraints [1–7]. A number of alternative technologies have been investigated for olefin production [8–24]. These are currently being viewed as more and more attractive given the increasing demands for ethylene and propylene. Oxidative dehydrogenation (ODH) is an alternate method for olefin production that does not suffer from the drawbacks of traditional methods. As an exothermic process, ODH can overcome the thermodynamic limitations of the non-oxidative dehydrogenation by formation of water, as a stable product. Moreover, ODH displays a large and positive equilibrium constant, decreasing at higher temperatures. Furthermore, the presence of oxygen limits coking and extends therefore catalyst usage. Moreover, light paraffins ODH can be operated at lower temperatures than either the thermal or the non-oxidative catalytic processes. So, ODH can thus offer potential increases in per-pass yields and energy savings while producing the desired olefins. Given that the formation of combustion products is thermodynamically favorable; selectivity control in ODH, reaction (1), is a major challenge. Undesired carbon oxides can be formed either by direct alkane combustion, reaction (2), or by deep oxidation of produced olefins, reaction (3). Thus, a catalyst for this reaction should be designed to prevent the undesirable reactions leading to carbon oxides [25–30].

Desired reaction:

$$C_2H_6 + 1/2O_2 \leftrightarrow C_2H_4 + H_2O \quad (1)$$

Undesired reactions:

$$C_2H_6 + (1.5 + x)O_2 \leftrightarrow 2CO_x + 3H_2O \quad (2)$$

$$C_2H_4 + (4x - 2)O_2 \leftrightarrow 2CO_x + 2H_2O \quad (3)$$

* Corresponding author. Tel.: +1 519 661 2144; fax: +1 519 850 2931.
E-mail address: hdelasa@fes.engga.uwo.ca (H. de Lasa).

0926-860X/$ – see front matter © 2012 Elsevier B.V. All rights reserved.
http://dx.doi.org/10.1016/j.apcata.2012.10.007

f_v	fraction of reduced vanadium metal
MW_V	molecular weight of vanadium
E_{des}	energy of desorption, kJ/mol
k_{d0}	pre-exponential factor
k_d	adsorption constant
T_m	centering temperature
T	desorption temperature, K
r_{des}	rate of desorption
V_d	volume of ammonia desorped, ml/g
V_m	volume of ammonia adsorbed at saturation conditions, ml/g
n	order of the desorption rate
R	the universal gas constant
VO_x	vanadium oxide surface species
$X_{C_2H_6}$	ethane conversion, %

Greek symbols

β	rate of temperature increase, °C/min
θ_{des}	surface coverage of adsorbed species
ν	stoichiometric number

Abbreviations

ODH	oxidative dehydrogenation
XRD	X-ray diffraction
TPR	temperature-programmed reduction
TPO	temperature-programmed oxidation
TPD	temperature-programmed desorption
DRIFTS	diffuse reflectance infrared Fourier transform spectroscopy
XPS	X-ray photoelectron spectroscopy

Vanadium-based catalysts have been reported in the technical literature as active and selective catalysts for ethane ODH [3,9,11,12,31–43]. This is due to the vanadium ability to provide lattice oxygen for hydrogen removal from alkanes, reaction (4) [25,44]. However, most of these studies involved co-feeding a gas phase molecular oxygen in order to re-oxidize the reduced metal oxides and replenish the lattice oxygen, reaction (5) [25,45]. However, in the present study ethane ODH is carried out in the absence of gas phase molecular oxygen.

$$C_2H_6 + MO_x \leftrightarrow C_2H_4 + H_2O + MO_{x-1} \quad (4)$$

$$MO_{x-1} + 1/2O_2(air) \leftrightarrow MO_x \quad (5)$$

The catalytic properties of vanadia can be improved by depositing it on appropriate metal oxide supports such as alumina, silica, titania, or zirconia. Variations in the catalytic performance of VO_x supported on metal oxides can be attributed to the formation of different VO_x species on the metal oxide support surfaces [27,29,33,46–51]. However, there is no clear relationship between the structure of surface vanadia species and their oxydehydrogenation using lower alkanes [33]. Furthermore, the catalytic activity and selectivity of supported vanadium oxide catalysts are significantly affected by the properties of the support material, the interaction of the surface VO_x species with the oxide support and the vanadium loading [29,33,38,46,48]. Alumina-supported vanadia has been considered in several structural investigations [12,29,33,36,52–57]. These studies showed that at low vanadium loading, a highly dispersed amorphous vanadate phase is formed. At medium loading, this phase's structure changes from isolated tetrahedral vanadium to polyvanadates species. However, a crystalline V_2O_5 phase was reported at high vanadium loading in addition to amorphous vanadia phases. Variations of the binding strength of surface lattice oxygen occur with the formation of different VO_x surface species structures. The binding strength has been proposed as the main parameter that governs activities and selectivities of alumina-supported vanadia catalysts [53,58].

While there is significant research on novel ODH catalysts [59–63], there is limited information that deals with light olefins ODH in dense fluidized beds, risers or downers reactors. These studies are confined to butane ODH [64–67]. Controlled isothermal conditions which are maintained in the catalytic fluidized beds are used. Hence, one circumvents with fluidized beds the potential issues with hot spots in fixed bed catalytic reactors. Non-isothermal conditions in fixed bed reactors can interfere with reactor performance and damage the catalyst.

Moreover, fluidized reactors with periodic catalyst re-oxidation offer the means that enable the transport of reduced catalyst species from the oxidative dehydrogenation unit (zone) to the re-oxidation unit (zone). Thus, the operation of twin reactors, one for the ODH and one for catalyst regeneration appear to be a requirement for the implementation of this technology at the industrial scale.

Given the above described facts, the goal for this paper is to provide in-depth research on the reactivity and stability of the prepared 10 wt.% VO_x/c-Al_2O_3 catalyst during ethane oxidative dehydrogenation. The 10 wt.% VO_x loading on the c-Al_2O_3 support was selected for this study to ensure that a sup-monolayer VO_x surface coverage is achieved (64.66% coverage). Several studies in the open literature have shown that supported vanadium catalyst are more active in ODH reactions with surface VO_x coverage in the sub-monolayer region [29,33,54,68–70]. Ethane ODH is performed in the present study under fluidized bed reaction conditions in the Chemical Reactor Engineering Center (CREC) Riser Simulator Reactor. Ethane was used as a feed for the ODH reaction and air was employed to regenerate the reduced catalyst sample.

2. Experimental

2.1. Catalyst preparation

The catalyst of this study was prepared by using the incipient wetness technique [43]. Vanadium oxide was supported on c-alumina (Alcan Activated Alumina AA-100, surface area of 260 m^2/g). Before the impregnation, the support particles were calcined at 500 °C for 4 h under a chromatographic quality air flow. Following this, the calcined support particles were impregnated at room temperature with a solution of V $(AcAc)_3$ in toluene prepared by dissolving 8 grams of V $(AcAc)_3$ precursor (Aldrich, 97%) in 100 ml toluene (0.153 M). After 24 h period of contact, the impregnated particles were filtered and separated from the supernatant liquid and the resulting cake was washed three times with fresh solvent. The resulting cake was dried first at 150 °C for 12 h. Then, the impregnated particles (catalyst precursor) were calcined under a GC quality air stream at 600 °C for a 6 h period.

Once the catalyst sample was prepared, the bulk amount of vanadium in the catalyst sample was determined using Atomic Absorption Spectroscopy. The prepared catalyst sample displayed a yellow-orange color showing a high concentration of V_2O_5 on the alumina surface (V^{5+}).

2.2. Catalyst characterization

2.2.1. BET surface area

The BET specific surface area analysis of the c-alumina support (237.90 m^2/g) and of the VO_x/c-alumina catalyst (205.80 m^2/g) were determined in a Micromeritics ASAP 2010 analyzer, by using nitrogen adsorption at 77 K. For each experiment, an amount of

0.26–0.30 g of catalyst sample was degassed at 350 °C for 2 h before analysis. The adsorption isotherms were measured in the 10^{-6} to 1 relative pressure range.

2.2.2. X-ray diffraction (XRD)

X-ray diffraction (XRD) analysis was used to identify the crystallographic structure of catalyst samples. XRD patterns of all catalysts reported in this study were recorded on a Rigaku MiniFlex Diffractometer with monochromatic Cu Kα radiation ($\lambda = 0.15406$ nm, 10 kV, 50 mA) using the normal scan rate of 2°/min. X-rays were collimated using a 1° divergent scattering slit, and a 0.15 mm receiving slit. Samples were scanned within the 2θ range of 20–80° with a step size of 0.02°.

2.2.3. Temperature programmed reduction (TPR)

Temperature programmed reduction (TPR) experiments were used to determine the degree of reduction of the catalyst and to reveal the temperature at which the reduction occurs. Moreover, TPR experiments were employed to assess the catalytic activity with frequent catalyst regenerations. It is known that the vanadium dispersion and the fractions of the different vanadia phases can change due to prolonged thermal treatment and after undergoing several reduction cycles [71]. It is likely that there is significant surface mobility of vanadia [72]. This can even cause changes in the nature of the surface species [73]. Therefore, the effect of the number of reduction and oxidation cycles on reducibility of vanadium oxide was also assessed by looking at the cyclic TPR/TPO experiments. TPR experiments were conducted using an AutoChem II ASAP 2920 analyzer, supplied by Micromeritics.

For TPR experiments, a fresh catalyst sample was pre-treated at 300 °C in a flow of high purity argon (99.9%) at a rate of 50 ml/min for 3 h. After cooling to ambient temperature, the argon flow was replaced by a reducing gas mixture (10.2% H_2/Ar) circulated at 50 ml/min. Then, the catalyst sample was heated in an argon atmosphere to 900 °C at a heating rate of 10 °C/min. Hydrogen concentration changes were determined in the outlet gas stream using a thermal conductivity detector (TCD). The area of the resulting peaks was integrated numerically, yielding the total hydrogen uptake volume.

2.2.4. NH_3 temperature programmed desorption (TPD)

NH_3-TPD was performed in the present study to determine the energy of desorption. This provided valuable insights on metal–support interactions assessing both TPD energetics and kinetics. Moreover, NH_3-TPD was used to determine the number and strength of acid sites available on the surface of the prepared catalyst samples.

NH_3-TPD experiments were conducted using the AutoChem II Analyzer from Micrometrics. For each experiment, the catalyst sample (between 0.274 and 0.281 g) was placed in a quartz container and degassed for 2 h at 300 °C in a flow of helium at 30 ml/min. The samples were then cooled to 100 °C and brought to saturation with ammonia using a NH_3/He gas mixture (4.55% NH_3/He) for one hour at a rate of 50 ml/min. After that, the ammonia flow was stopped, and replaced by a He purge gas, fed at the rate of 50 ml/min. This was done for 1 h at 100 °C to remove the physically adsorbed ammonia. Following this step, the temperature was raised up to 500 °C at different heating rates (5, 10, 20 and 30 °C/min). As the temperature was increased, ammonia desorbed as it gained enough energy to overcome the activation energy barrier.

2.3. Reactivity and stability test in the CREC Riser Simulator

The reactivity and the stability of the VO_x/Al_2O_3 catalyst were established using the CREC Riser Simulator. The CREC Riser Simulator is a bench scale mini-fluidized bed reactor, invented by de Lasa [74] at Chemical Reactor Engineering Center (CREC), Western University. This mini-fluidized reactor (capacity of 53 cm^3) is a batch unit designed for catalyst evaluation and kinetic studies under fluidized bed (riser/downer) reactor conditions. One of the main advantages of this unit is its capability of simulating fluidized bed reactions conditions by using a very small amount of catalyst. The main reactor consists of a lower shell and an upper shell. These two shells allow easy access to the reactor in order to load and unload catalyst samples. The lower shell houses a basket that contains the catalyst sample. The catalyst is held in place in the reactor basket by two porous grids placed at each end of the basket. An impeller is located above the reactor basket and upon rotation of the impeller at high speed (up to 7000 rpm) reactant gas is withdrawn through the basket causing the solid catalyst to become fully fluidized.

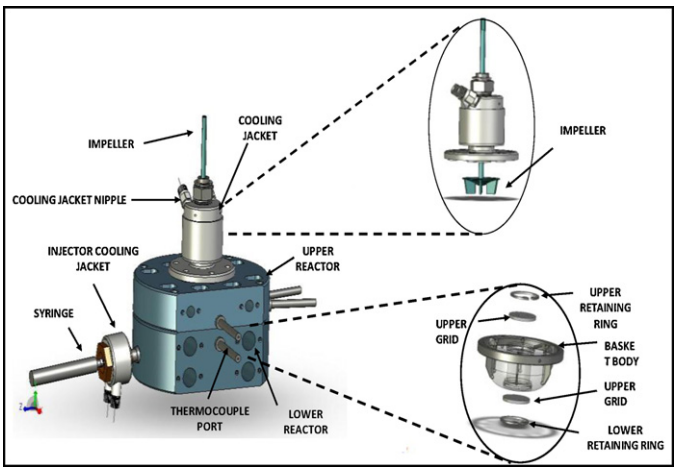

Fig. 1. Overview of the CREC Riser Simulator reactor body.

A schematic diagram of the CREC-Riser Simulator reactor body is provided in Fig. 1. The CREC Riser Simulator operates in conjunction with some other accessories, such as a vacuum box, a gas chromatograph (GC), and series of sampling valves, a timer, two pressure transducers and two temperature controllers. A schematic diagram of the CREC Riser Simulator experimental set-up used in this study is shown in Fig. 2.

For each reaction run, the required amount (maximum 1 g) of catalyst sample was first loaded into the reactor basket and then the reactor was closed. The temperature program was run to heat up the system to the desired reaction temperature. An argon flow was maintained in the system to ensure that the system was free from

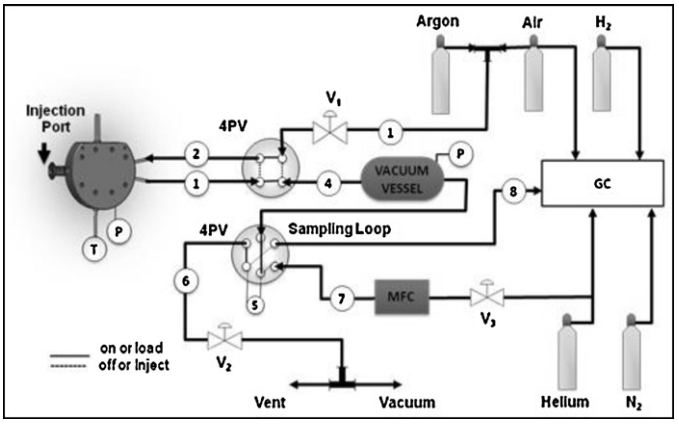

Fig. 2. Schematic diagram of the CREC Riser Simulator experimental set-up.

Table 1
Characteristics of alumina support and supported vanadia catalyst.

Sample	V content (wt.%)[a]	Surface area (m^2/g)
Activated Al_2O_3	–	237.9
V_2O_5/Al_2O_3	10	205.8

[a] Vanadium content, in wt.% of V atoms, was determined by ICP.

any gaseous oxygen (air). Once the reactor reached thermal equilibrium at the desired temperature, the argon flow was stopped and the vacuum box pressure was reduced to 20.7 kPa using a vacuum pump. At this stage, the impeller was turned on and the feed (C_2H_6) was injected into the reactor using a preloaded syringe. During the reaction period, the pressure profile of the reactor was recorded using a pressure transducer. The reactor pressure increased as soon as the reaction proceeded, given the increased number of moles in the gas phase due to the ODH reaction. At the end of the prespecified reaction time, the isolation valve between the reactor and the vacuum box was opened and the pressure was reduced to the value of the vacuum box pressure. The sudden decrease of the reactor pressure ensured that most of the reactant/product was removed from the reactor almost instantaneously and that no further reaction took place. Finally, the product gas was analyzed by means of an on-line GC (Shimadzu-2010) equipped with a 60/80 Carboxen-1006 packed column, a thermal conductivity detector (TCD) and a flame ionization detector (FID). The concentrations of the following gases were determined: CO, CO_2, C_2H_4 and C_2H_6.

3. Results and discussion

3.1. Catalyst characterization

Fluidizable c-$A1_2O_3$ was selected as the support material for vanadium oxide given its thermal and mechanical stability under the selected reactor conditions. The BET surface area for the support material and for the metal loaded catalyst sample is shown in Table 1. The surface area of the bare commercial c-$A1_2O_3$ is in good agreement with the value given by the supplier (230 m^2/g). A moderate decrease is noticed in the total surface area of the catalyst after vanadium loading on the calcined c-$A1_2O_3$ support. This decrease in surface area is attributed to the plugging of some of the support pores by the vanadium species.

3.1.1. X-ray diffraction (XRD)

The X-ray powder diffraction patterns of the fresh VO_x/c-Al_2O_3 catalyst and activated commercial c-Al_2O_3 support samples are shown in Fig. 3. The diffraction patterns of bulk V_2O_5 is also shown as a reference (case A in Fig. 3). For the activated c-Al_2O_3 sample, there were no diffraction peaks except at $2\theta = 78^\circ$, which is the characteristic peak for the c-Al_2O_3 phase (case C in Fig. 3). Moreover, no changes in the XRD patterns were observed on the VO_x-loaded c-Al_2O_3 support (case B in Fig. 3). The absence of the peaks at this VO_x loading can be taken as an indication of the absence of V_2O_5 bulk surface species and that VO_x phase is primarily present as an amorphous phase consisting of monovanadate or polyvanadates surface species. These observations are in agreement with the published data [12,29,36] on supported vanadia catalysts with similar VO_x loadings on c-Al_2O_3 supports. According to these studies, the VO_x phase is primarily present as vanadate or polyvanadate, which is known to be X-ray amorphous. Moreover, XRD also shows that no other species is formed due to the interaction between the V_2O_5 catalyst and the Al_2O_3 support.

3.1.2. Temperature programmed reduction and oxidation

Fig. 4 reports consecutive TPR profiles for the VO_x/c-Al_2O_3 catalyst sample. It can be noted that the prepared catalyst showed very stable reduction behavior during consecutive TPR cycles. TPR experiments display a single reduction peak in each TPR cycle extending from 310 °C to 600 °C with a T_{max} at 550 °C for the 5th TPR cycle. These results show that repeated TPR–TPO cycles do not alter the reducibility of the supported V-species. In agreement with this, minor variations were observed in terms of the H_2 gas consumption during various TPR cycles. Moreover, it was shown that the TPR cycles were consistently completed when the temperature was at 600 °C. Furthermore, there was no additional higher temperature reduction peak, which is a characteristic in the reduction of bulk-like V_2O_5 species. The same result was also confirmed by the XRD analysis as there was no diffraction patterns observed in the crystalline phase of the V_2O_5 species catalyst surface.

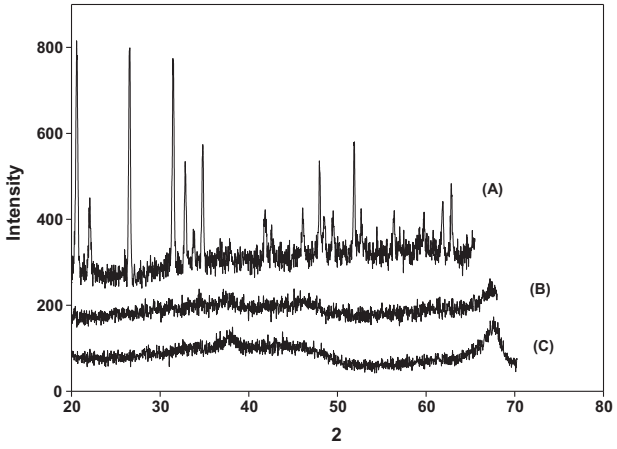

Fig. 3. XRD results for the following cases: (A) bulk V_2O_5 sample, (B) fresh 10 wt.% V_2O_5/c-Al_2O_3 catalyst sample, and (C) activated Al_2O_3 support sample.

The XRD pattern for catalyst sample following the 5 TPR/TPO cycles (case B) is compared with that for fresh catalyst sample (case A) in Fig. 5. The absence of any reflection peaks corresponding to crystalline VO_x phase confirmed the stable behavior of the sample and maintaining a consistent metal dispersion during the successive oxidations and reduction in consecutive TPR/TPO cycles. Moreover, this can be taken also as an indication of the absence of metal sintering (metal crystallite agglomeration).

The degree of reduction of the catalyst can be defined as the ratio of the exposed reducible vanadium oxide over the total vanadium oxide amount in the catalyst. The amount of exposed reducible vanadium on the catalyst sample can be related to the amount of hydrogen consumed during the reduction process. Thus, the

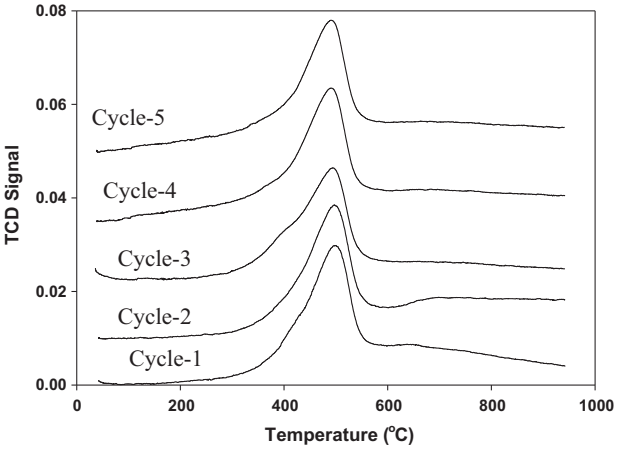

Fig. 4. Successive TPR profiles for VO_x/c-Al_2O_3 catalyst. Pre-treatment: calcination at 773 K.

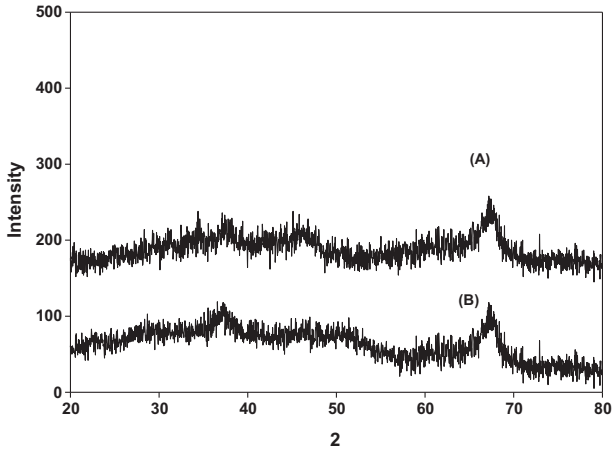

Fig. 5. XRD patterns for the following cases: (A) fresh 10 wt.% V_2O_5/c-Al_2O_3 catalyst sample and (B) spent 10 wt.% V_2O_5/c-Al_2O_3 catalyst sample after 5 TPR/TPO cycles.

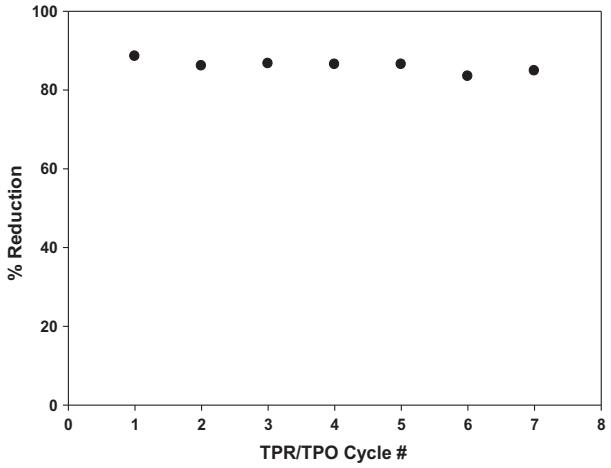

Fig. 6. Degree of reduction of Al_2O_3-supported VO_x catalyst sample in multiple TPR/TPO cycles up to 950 °C (heating rate: 10 °C/min; reducing agent: 10% H_2/Ar at 50 cm^3/min; oxidizing agent: 5% O_2/He at 50 cm^3/min).

amount of reacted hydrogen is established by numerically integrating the area of the resulting TPR peak. This allows the amount of reducible metal in the catalyst sample to be calculated using the following equation:

$$W_V = \frac{MW_V \times V_{H_2}}{\nu \times V_g} \quad (6)$$

where (a) W_V is the amount of reduced vanadium (g), (b) MW_V is the molecular weight of vanadium (g/mol), (c) V_{H_2} is the volume of reacted hydrogen (cm^3 at STP), (d) V_g is the molar volume of gas (mol/cm^3 at STP). (e) ν is the stoichiometric number of hydrogen based on the following reaction stoichiometry.

Assuming that V_2O_5 is the initial reducible catalyst species present on the support, then:

$$V_2O_5 + 2H_2 \rightarrow V_2O_3 + 2H_2O$$

Thus, by knowing the amount of reducible metal in the catalyst sample, W_V, and by knowing the actual vanadium amount on the catalyst, W_0, the fractional amount of reducible vanadium (% reduction) can be calculated using the following equation:

$$f_V = \frac{W_V}{W_0} \quad (7)$$

The effect of the number of TPR/TPO cycles on the reducibility of the supported vanadium oxide catalyst was also assessed from cyclic TPR/TPO experiments. Fig. 6 reports the reducibility (% reduction) of the VO_x/c-Al_2O_3 catalyst sample used in this study under repeated TPR/TPO cycles. On this basis, it can be concluded that approximately 85% reduction was achieved in each cycle assuming that V_2O_5 was the initial phase of VO_x on the catalyst sample. The sequence of TPR/TPO cycles demonstrates that there is a consistent percentage reduction of V_2O_5. This indicates that the sample is stable over repeated reduction/oxidation cycles. This observation suggests that no phase transformation takes place during the redox cyclic process up to 950 °C.

3.1.3. Catalyst total acidity

Ammonia is a well known probe molecule used to characterize acidic properties of solid catalysts. This is due to ammonia's strong basicity as well to its small molecular size. Ammonia allows the determination of acidic sites within a wide range of catalyst pore sizes [75]. Thus, the total acidity of the catalyst sample can be determined by the total amount of ammonia adsorbed/desorbed.

In this study, the saturation of the VO_x/c-Al_2O_3 catalyst sample and the bare c-Al_2O_3 support were carried out at different saturation temperatures. The amount of ammonia adsorbed/desorbed

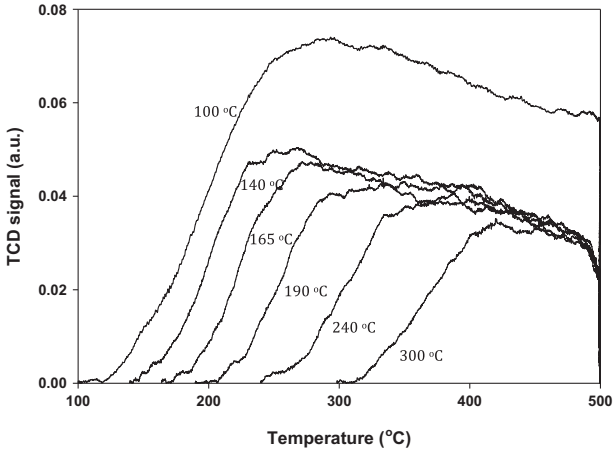

Fig. 7. NH_3-TPD spectra at various temperatures of ammonia adsorption on VO_x/c-Al_2O_3 catalyst sample (β = 30 °C/min).

by the catalyst sample was calculated from the ammonia desorption peaks as shown in Fig. 7 and Table 2. As listed in Table 2, the total ammonia desorption of both samples decreased with increasing saturation temperature. This was the case when the selected saturation temperature was above 200 °C. Thus, this shows that 200 °C is too high of a thermal level to achieve complete ammonia saturation for all the available acid sites on the sample surface.

NH_3-TPD was also used in this study to compare the total acidity and acid strength of the bare c-Al_2O_3 support, to the fresh and reduced (after reaction) VO_x/Al_2O_3 catalyst samples as shown in Fig. 8 and Table 3. Table 3 shows that the prepared 10 wt.% VO_x/c-Al_2O_3 catalyst displays a considerably lower acidity while compared to that of the bare alumina support. The vanadium loading on the c-$A1_2O_3$ support reduces the acidity of bare c-$A1_2O_3$, from 14.39 ml NH_3/g to 6.77 ml NH_3/g. This acidity reduction can

Table 2
Amount of ammonia desorbed (in ml/g sample) at different adsorption temperatures (β = 30 °C/min, sample weight: 0.274 g).

Sample	NH_3 adsorption temperature (°C)					
	100	140	165	190	240	300
c-Al_2O_3	14.39	12.63	11.02	9.80	6.82	4.49
VO_x/c-Al_2O_3 (fresh)	6.77	5.69	4.45	3.91	3.34	2.29

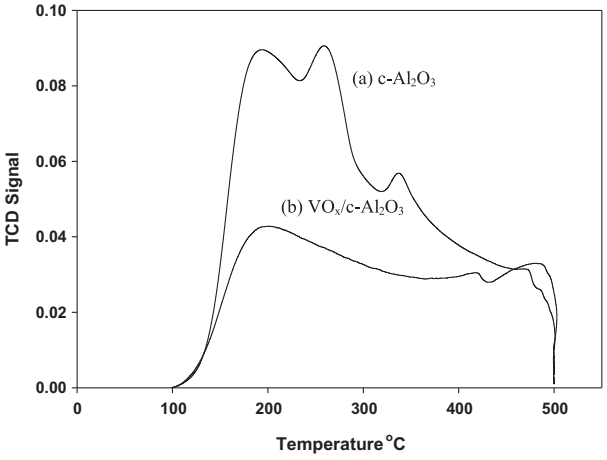

Fig. 8. NH_3-temperature programmed desorption profiles for (a) c-Al_2O_3 support, (b) fresh 10 wt.% VO_x/c-Al_2O_3 catalyst (β = 30 °C/min: 15 °C/min, NH_3 pre-adsorbed at 100 °C).

be attributed to the coverage of acid sites by VO_x surface species on the alumina surface. Desorption peaks reported in Fig. 8 at 180 °C for bare Al_2O_3 support are attributed to the desorption of NH_3 from weak acid sites, while higher temperature peaks at 345 °C and 365 °C are assigned to the desorption of NH_3 from medium to stronger acid sites respectively. After VO_x loading however, the supported VO_x catalyst samples showed only one desorption peak at 200 °C which is similar to the one for the bare support. This result suggests that the loading of VO_x species on the Al_2O_3 support affect acid sites number as follows: (a) the strong acid site number remain close, (b) the weak acid sites are significantly reduced. Similar results are reported in the literature on the acidity of supported-vanadia catalysts [76,77]. It was concluded in these studies that the formation of the surface vanadia species on oxide supports such as c-Al_2O_3 is accompanied by the surface coverage of c-Al_2O_3 acid sites with VO_x species.

3.1.4. TPD kinetics and heat of desorption

In order to characterize the desorption behavior and relate the NH_3-TPD results with fundamental desorption kinetics; the TPD data were further analyzed. This was done to determine the desorption energy and frequency factors. This was accomplished through the setting up of a desorption model. It was tested against experimental data by curve fitting. The rate of desorption at a constant activation energy, as described by Cvetanovic and Amenomiya [78], was used in order to determine the desorption parameters from the NH_3-TPD results. In order to apply this model, the following assumptions were made:

(i) The surface of the catalyst is homogeneous for the adsorption of ammonia, that is, $k_d = k_{d0}\exp(-E_{des}/RT)$, with k_d being independent of the surface coverage (θ_{des}).
(ii) Readsorption of the desorbed NH_3 gas does not occur.
(iii) There is a uniform concentration of the adsorbate in the gas phase through the catalyst bed.
(iv) The desorption rate is of first order in coverage.
(v) Linear temperature increases with time.

Table 3
Temperature programmed desorption of NH_3 for Al_2O_3 and VO_x/Al_2O_3 catalysts.

Catalyst sample	T_{des} (°C)	Total NH_3 uptake (ml STP NH_3/g)
c-Al_2O_3	180, 265, 340	14.39
VO_x/c-Al_2O_3	200	6.77

The NH_3-TPD experimental conditions were chosen to ensure that the assumption (ii) was satisfied by maintaining a high gas flow through the catalyst bed. This was done to prevent the readsorption of the desorbed species. Similarly, assumptions (iii) and (v) were considered satisfied in the experiments by selecting appropriate experimental conditions. Moreover, assumption (iv) was considered appropriate given that ammonia desorption was unimolecular [79].

Thus, the rate of NH_3 desorption at a constant activation energy for first order desorption can be obtained by performing a species balance of desorbing ammonia species as considered by Farrauto and Bartholomew [80]; White [81]; Tonetto et al. [79] and Sedor et al. [82]:

$$r_{des} = -V_m\left(\frac{d\theta_{des}}{dt}\right) = k_{d0}\theta_{des}\exp\left(-\frac{E_{des}}{R}\left(\frac{1}{T}-\frac{1}{T_m}\right)\right) \quad (8)$$

where θ_{des} is the surface coverage of the adsorbed species, K_d is the desorption constant, k_d is a pre-exponential factor, E_{des} is the activation energy of desorption and T_m is the centering temperature, which minimizes the cross-correlation between parameters.

In a TPD experiment, the temperature of the bed is raised linearly at a constant heating rate, β, as given by:

$$T = T_0 + \beta t$$

And thus:

$$\frac{dT}{dt} = \beta \quad (9)$$

And given that:

$$\left(\frac{d\theta_{des}}{dt}\right) = \left(\frac{d\theta_{des}}{dT}\right)\left(\frac{dT}{dt}\right) = \beta\left(\frac{d\theta_{des}}{dT}\right) \quad (10)$$

As a result, Eqs. (8) and (10) yield the following equation,

$$\left(\frac{d\theta_{des}}{dT}\right) = -\frac{k_{des0}}{V_m\beta}\theta_{des}\exp\left(-\frac{E_{des}}{R}\left(\frac{1}{T}-\frac{1}{T_m}\right)\right) \quad (11)$$

where:

$$\theta_{des} = 1 - \frac{V_{des}}{V_m} \quad (12)$$

Substituting Eq. (12) into Eq. (11) and after the required mathematical rearrangement, the variation of the desorbed volume of ammonia with temperature (dV_{des}/dT) can be expressed as a function of desorption as:

$$\frac{dV_{des}}{dT} = \frac{k_{des0}}{\beta}\left(1-\frac{V_{des}}{V_m}\right)\exp\left(-\frac{E_{des}}{R}\left(\frac{1}{T}-\frac{1}{T_m}\right)\right) \quad (13)$$

Using Eq. (13), the energy of ammonia desorption and the pre-exponential factor can be estimated. To accomplish this, a non-linear regression analysis was carried out using the MATLAB numerical computing software with experimental TPD data obtained at various linear heating rates (β = 7, 10, 15, 20 and 30 °C/min). In addition, the differential equation (Eq. (13)) was solved using the ODE 45 (in MATLAB, 4th order Runge–Kutta) least squares method. Both k_{des0} and E_{des} parameters were estimated to be in the 95% confidence interval. The regression analysis was considered converged when the model function value changed less than the specified tolerance of 10^{-8}.

In all of the experiments for the NH_3-TPD kinetics study, the catalyst samples were saturated by flowing ammonia (50 ml/min) at 100 °C first. This was the case given that 100 °C yielded the highest amount of ammonia adsorbed/desorbed. Following this, the saturated samples were heated at different linear heating rates of 5, 10, 20, and 30 °C/min. In each case, the desorption rate against desorption temperature was recorded as shown in Fig. 7.

Table 4
Estimated parameters for NH_3-TPD kinetics (adsorption at 100 °C).

Sample	B (°C/min)	E_{des} (kJ/mol)	k_{des0} (cm^3/min)	R^2	γ	V_{NH_3} (ml/g)	Degree of freedom n = data points − 2
c-Al_2O_3	5	13.31 ± 0.41	7.98×10^{-3} ± 0.12	0.995	0.520	13.30	408
	10	14.81 ± 0.44	8.60×10^{-3} ± 0.11	0.996	0.653		213
	20	16.55 ± 0.45	0×10^{-3} ± 0.10	0.994	0.752		218
	30	15.00 ± 0.56	6.50×10^{-3} ± 0.13	0.995	0.787		308
	All data	14.42 ± 0.52	$8.32 \times 10-3$ ± 0.13	0.995	0.698		1147
VO_x/c-Al_2O_3	5	17.09 ± 0.27	3.00×10^{-3} ± 0.05	0.993	0.749	5.93	381
	10	18.80 ± 0.27	3.20×10^{-3} ± 0.05	0.996	0.748		224
	20	18.24 ± 0.15	2.70×10^{-3} ± 0.01	0.997	0.799		127
	30	19.38 ± 0.21	2.40×10^{-3} ± 0.01	0.996	0.837		229
	All data	17.96 ± 0.20	$3.22 \times 10-3$ ± 0.03	0.996	0.771		961

β, heating rate; E_{des}, activation energy of desorption; γ, cross-correlation coefficient; V_{NH_3}, total ammonia adsorbed/desorbed.

Table 4 reports the estimated energy of desorption for the prepared 10 wt.% VO_x/c-Al_2O_3 catalyst sample and the bare c-Al_2O_3 support. Statistical criteria such as degree of freedom, the 95% confidence intervals, correlation coefficient (R^2) and cross-correlation between parameters are considered in the analysis. As can be seen in Table 4 a close to one value is found for the R^2 correlation coefficient, a necessary condition for proposed desorption model applicability. In addition, both energy of desorption (E_{des}) and intrinsic kinetic parameters (k_{des0}) display narrow spans for the 95% confidence interval. Moreover, minimum interaction between the estimated parameters is observed given the low c cross-correlation coefficients reported. These favorable indicators are accompanied by good agreement between the experimental data and the proposed desorption model.

One can see in Table 4 that the estimated activation energies for each sample are in agreement at various heating rates (5, 10, 20, 30 °C/min). Furthermore, when all the TPD data points were considered for kinetic modeling, they showed consistent estimated energy of desorption while compared to the ones obtained for the individual heating rates as also shown in Table 4.

The fitting of the model using Eq. (13) as well as the experimental TPD data are reported in Fig. 9. Furthermore, in Fig. 9, it can be noted that a good agreement exists between the calculated values using the proposed model and the experimental values. These further support the validity of the proposed model.

When comparing the bare c-Al_2O_3 support and the vanadium loaded VO_x/c-Al_2O_3 catalyst, it can be noticed that the energy of activation slightly increased after vanadium loading on the alumina support. The activation energy of ammonia desorption for the bare c-Al_2O_3 support was found to be 14.42 kJ/mol. After vanadium loading, the value increased to 17.96 kJ/mol.

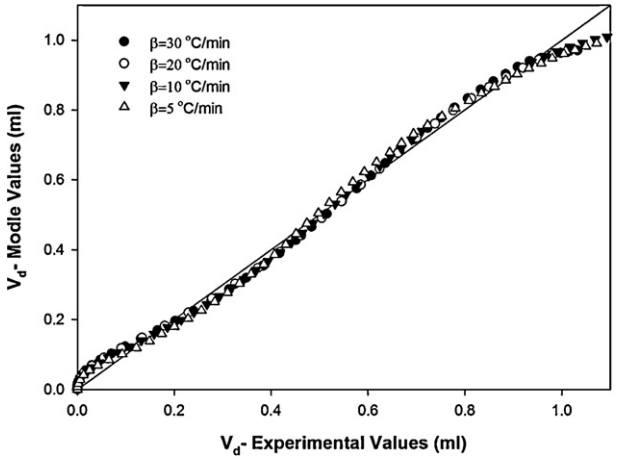

Fig. 9. Experimental data and fitted model (Eq. (13)) of ammonia desorption during NH_3-TPD at different heating rates on VO_x/c-Al_2O_3 catalyst (NH_3 adsorbed at 100 °C). *Note*: reported points are one every 30 s to avoid overlapping of the data points. The original data file includes data points taken every 2 s and as a result more than 300 data points are available for the parameter estimation.

This change in the estimated activation energy can be related to the total ammonia desorbed from the bare alumina support and from the catalyst sample as seen in Table 2. At similar conditions, the total amount of ammonia adsorption/desorption is significantly higher in the case of the bare c-Al_2O_3 support. This means that there is a smaller activation energy of ammonia desorption for the bare c-Al_2O_3 support.

Similar observations were reported by Alvarez-Merino et al. [83] on activated carbon supported tungsten catalysts where lower desorption energy corresponded to higher amounts of ammonia desorption from the catalyst samples. This slight increase in desorption activation energy for the VO_x/c-Al_2O_3 catalyst when compared with the bare alumina support points toward the extent to which the metal–support interactions are present. The increase of activation energy of desorption for supported metal catalysts can be related to the change of heterogeneity of the catalyst due the interaction between the active metal sites and the support [75]. In a study by Farrauto and Bartholomew [80] on H_2-desorption using on Ni/Al_2O_3 samples, higher activation energy of desorption was reported for Ni-loaded catalysts when compared to the bare alumina support. This was attributed to the local interaction between the nickel on aluminum oxide species. In the context of this study, only a slight increase in desorption activation energy was observed when using the V-loaded catalyst sample. Hence, it can be concluded that there is weak metal–support interaction in the prepared 10 wt.% VO_x/c-Al_2O_3 catalyst. Hence, this gives, a well dispersed catalyst with lattice oxygen readily available for the ODH reaction.

The same conclusion can be reached by using the XRD pattern of the prepared VO_x/c-Al_2O_3 catalyst. In fact, the XRD do not show peaks other than the ones for the alumina support. This indicates that no other crystalline species such as vanadium-aluminates are formed as a result of the interaction between VO_x and Al_2O_3 support.

3.2. Ethane ODH experiments in the CREC Riser Simulator

Catalytic experiments of ethane ODH in the CREC Riser Simulator were carried out using pure ethane feed (Paraxair 99.99%) at atmospheric pressure. The temperatures and reaction times were varied between 550–700 °C and 10–40 s, respectively. One loading of catalyst (0.76 g) was used throughout the study. The VO_x/c-Al_2O_3 catalyst sample was fluidized in the riser basket where the reduction reaction took place. Every reaction set consisted of catalyst reduction cycles using ethane as a feed. This was followed by catalyst regeneration in air at 525 °C for 10 min.

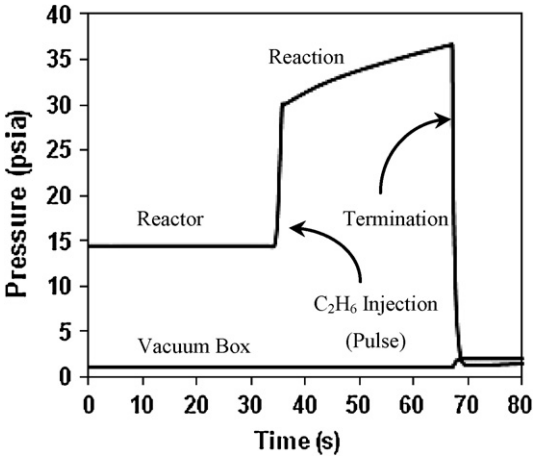

Fig. 10. Pressure profile in the CREC Riser Simulator during ethane ODH.

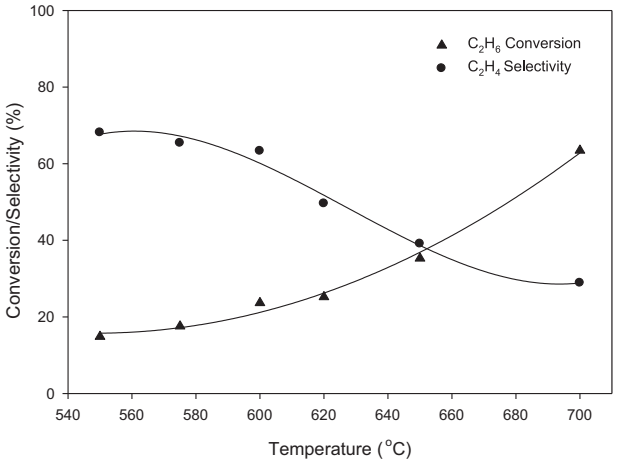

Fig. 11. Temperature dependence of C_2H_6 conversion and C_2H_4 selectivity (reaction time = 30 s, C_2H_6 injected = 20 ml, catalyst loaded = 0.76 g). Ethane conversions and ethylene selectivities reported are for the tenth consecutive ethane injection (pulse).

During each ethane ODH run performed in the CREC Riser Simulator, the pressure was monitored at the injection (pulse), reaction and termination of the run. Typical pressure profiles during each ethane ODH run are reported in Fig. 10. The upper curve of Fig. 10 displays an increase in total pressure from injection (pulse) time to termination time. This pressure rise is due to the increase in the total number of moles. During this time, the reaction between the ethane and the lattice oxygen takes place.

The lower curve in Fig. 10 represents the pressure profile in the vacuum box, which remained constant during the reaction period. At termination time, and due to the gaseous products transferred from the reactor to the vacuum box, the reactor pressure abruptly decreases while the vacuum box pressure slightly increases.

As a result, reaction products are contained in the vacuum box preventing any further reaction, and are ready for the GC analysis. The product analysis shows that both CO_2 and CO are products of combustion and of partial combustion of ethane, respectively.

The experimental results of ethane oxidative dehydrogenation using the prepared $VO_x/c\text{-}Al_2O_3$ catalyst at various temperatures are reported in Table 5. The only identifiable carbon products other than ethylene were CO, CO_2 and C_2H_4 with this showing that there is no evidence of ethane coupling to higher hydrocarbons.

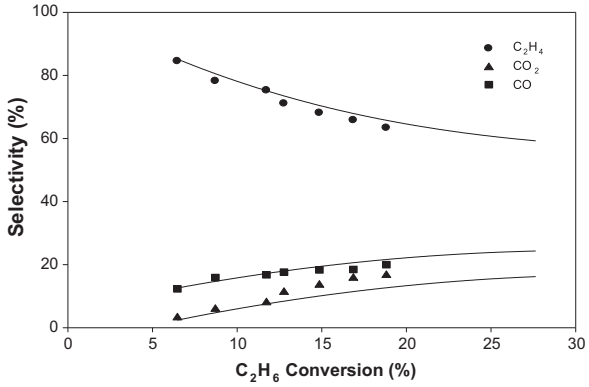

Fig. 12. C_2H_6 CO and CO_2 selectivities as a function of C_2H_6 conversion (T = 550 °C, C_2H_6 injected = 20 ml, catalyst loaded = 0.76 g). Ethane conversions and ethylene selectivities reported are for the tenth consecutive ethane injection (pulse).

3.2.1. *Effect of temperature*

For ethane ODH in the CREC Riser Simulator, the reaction temperatures were varied between 550 and 700 °C. The relationships

Table 5
Catalytic results for the oxidative dehydrogenation of ethane on $VO_x/c\text{-}Al_2O_3$ catalyst for the tenth consecutive ethane injection (pulse).

Temperature (°C)	Reaction time (s)	X_{ethane} (%)	Selectivity (%)				C_2H_4 yield (%)
			C_2H_4	CO_2	CO	CO_x	
550	10	6.47	84.51	3.18	12.32	15.49	5.47
	15	8.72	78.21	5.89	15.90	21.79	6.82
	20	11.73	75.25	7.96	16.78	24.75	8.83
	25	12.77	71.08	11.28	17.64	28.92	9.07
	30	14.86	68.12	13.55	18.34	31.88	10.12
	35	16.86	65.80	15.73	18.47	34.20	11.10
	40	18.82	63.38	16.64	19.99	36.62	11.93
575	10	7.65	83.82	2.88	13.31	16.18	6.41
	15	10.85	78.55	5.06	16.39	21.45	8.52
	20	12.77	72.30	7.83	19.86	27.70	9.23
	25	15.32	68.69	10.07	21.24	31.31	10.52
	30	17.56	65.39	12.28	22.33	34.61	11.49
	35	19.87	65.21	12.80	21.99	34.79	12.96
	40	21.59	62.34	14.69	22.97	37.66	13.46
600	10	11.84	79.42	3.92	16.66	20.58	9.41
	15	15.53	75.30	6.51	18.19	24.69	11.70
	20	18.05	67.44	9.33	23.23	32.56	12.17
	25	21.17	64.59	11.36	24.04	35.41	13.68
	30	23.67	63.30	13.44	23.26	36.70	14.98
	35	25.84	61.80	15.11	23.08	38.20	15.97
	40	27.64	57.62	17.80	24.80	42.38	15.93

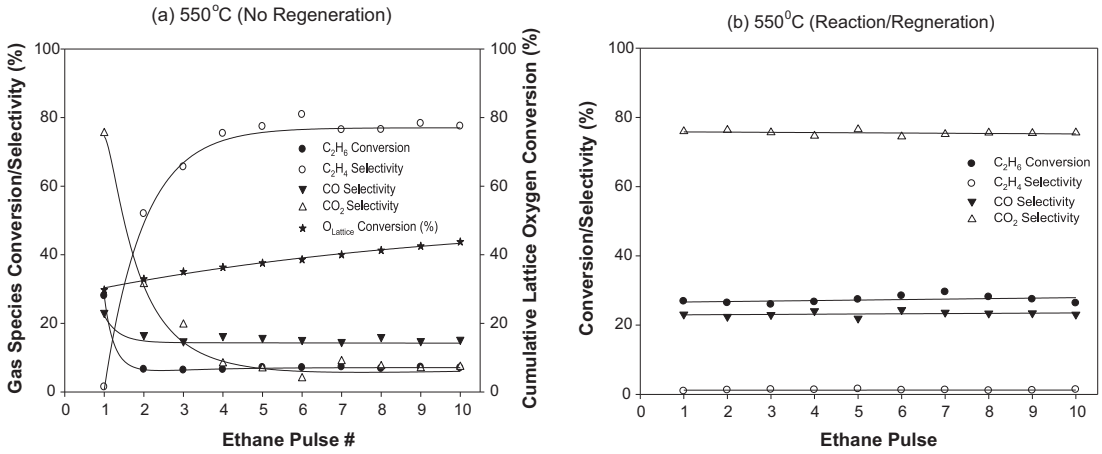

Fig. 13. Ethane conversion, ethylene, CO, CO_2 selectivities and cumulative lattice oxygen conversion using a VO_x/c-Al_2O_3 catalyst in the CREC Riser Simulator (T = 550 °C, C_2H_6 injected = 20 ml, reaction time = 15 s, catalyst loaded = 0.76 g) (a) Consecutive ODH runs without catalyst re-oxidation in between ethane pulses and (b) consecutive ODH runs with catalyst re-oxidation in between ethane pulses.

between ethane conversion and ethylene selectivity with reaction temperature are shown in Fig. 11.

It can be seen that as the reaction temperature increases, the conversion of ethane is raised from 14.86% at 550 °C to 63.46% at 700 °C. On the other hand, selectivity to ethylene showed a slight decrease from 68.12% at 550 °C to 63.29% at 600 °C. This was followed by a further gradual decrease to 28.86% with increasing temperature to 700 °C. This type of relationship is expected as ethane conversion due to cracking tends to become more dominant at higher temperatures. Hence, more by-products are favored at the expense of ethylene selectivity. As the test results show, an increase in temperature improves ethane conversion. On the other hand, it decreases selectivity toward the desired ethylene product. Therefore, a careful selection of an appropriate reaction temperature is critical for meeting the objectives of both the desired yield and selectivity.

To shed light into the reaction network, experiments were performed at various contact times. The selectivity of products for ethane ODH as a function of the conversion of ethane is illustrated in Fig. 12. Ethylene appears as the primary reaction product of the ethane ODH. The decrease in ethylene selectivity with a corresponding increase in CO and CO_2 selectivities indicates that CO and CO_2 are the secondary products of consecutive oxidation of ethylene.

3.2.2. Ethane ODH cycles

Having obtained encouraging results in the CREC Riser Simulator and to be able to assess catalyst stability, the prepared VO_x/c-$A1_2O_3$ catalyst was evaluated over multiple ODH runs through consecutive ethane reaction cycles.

Fig. 13a reports ethane conversion and products selectivity for consecutive ethane reaction cycles with no catalyst regeneration in between ethane injections (pulses). It can be observed that the ethane conversion is a function of the number of ethane injections (pulses) at 550 °C. In this set of experiments, the catalyst supplies oxygen removing hydrogen and forming ethylene and water. During the first reaction cycle (first injection or first pulse), ethane conversion was 43.1% with 0.94%, 23.1% and 75.9% selectivities for ethylene, CO and CO_2, respectively. These product selectivities at this ethane conversion can be related to the excess oxygen available in the fresh catalyst. This excess oxygen is likely to favor the conversion of methane into combustion products. This is apparent from the low C_2H_4 selectivity and the high combustion product selectivities obtained.

However, following the first reaction cycle (first injection or first pulse), ethane conversion showed a sharp decrease to 6.47%. This was accompanied with a sudden increase in ethylene selectivity to 84.51%. At the same time, CO and CO_2 selectivities decreased to 12.32% and 3.18%, respectively. In the subsequent runs however, ethane conversion displayed a gradual reduction to 0.817%. This trend was accompanied with a progressive increase in ethylene selectivity up to 96.01% and a decrease in CO and CO_2 selectivities to 3.86% and 0.12%, respectively.

These findings prove that in consecutive ODH reactions without catalyst regeneration in between (oxygen-free environment), ethane can be converted selectively to ethylene. This occurs due to the lattice oxygen involvement in the ODH reaction mechanism. One can also notice that following the first ethane injection (first pulse), the catalyst tested displays a stable performance in terms of ethane conversion and ethylene selectivity even after ten repeated reduction runs [84].

Fig. 13b reports a second set of experiments involving ethane ODH reactions using the same VO_x/c-Al_2O_3 catalyst, 550 °C and repeated reaction–regeneration cycles. Catalyst regeneration was conducted by flowing air at 550 °C over the catalyst after each ethane injection (pulse) or ODH reaction cycle. Results show that ethane conversions and product selectivity remain stable during the different runs with the following trends observed: (a) ethane conversion staying at the 43.5% level, (b) ethylene selectivity being close to 1.5%, (c) CO and CO_2 selectivities remaining at 23.5% and 75.5%, respectively. Ethylene, CO and CO_2 selectivities are in clear contrast with the ones reported in Fig. 13a and show that formation of the CO and CO_2 is promoted by gas phase oxygen.

In conclusion, the performance of the 10 wt.% VO_x/c-alumina catalyst of the present study is affected considerably by both ODH operation conditions and catalyst regeneration. It appears that consecutive reaction injections (pulses) are a preferred mode of operation for ODH. Regeneration shall only be allowed once this series of consecutive reaction cycles is completed.

One can, for instance, envision that this is equivalent to operating a twin circulating fluidized reactor process (reactor–regenerator), where the following occurs: (a) most of the catalyst stream leaving the reactor is returned to the ODH unit directly; (b) only a small fraction of the catalyst stream is directed toward the regenerator. This operational strategy can allow the functioning of industrial scale ODH processes with high ethylene selectivities, under conditions close to the ones reported in Fig. 13a.

4. Conclusions

The following are the relevant conclusions of the present study:

(i) TPR results demonstrate that the prepared 10 wt.% VO_x/c-alumina catalyst is stable over repeated reduction and oxidation cycles with the reduction temperature being around 550 °C.

(ii) XRD shows the absence of V_2O_5 bulk surface species and the high dispersion of VO_x on the support surface. XRD results are in agreement with the published literature on c-Al_2O_3 supported vanadia catalysts with similar VO_x loadings. The VO_x phase is primarily present as amorphous vanadate or polyvanadate. Moreover, XRD also shows that no species is formed due to the interaction between V_2O_5 and the Al_2O_3 support.

(iii) NH_3-TPD proves that vanadium addition on c-Al_2O_3 reduces the acidity of bare c-Al_2O_3, from 14.39 ml NH_3/g to 6.77 ml NH_3/g.

(iv) NH_3-TPD allows calculating energies of desorption. One can notice a slight increase in the desorption energy for the VO_x/c-Al_2O_3 catalyst versus the one for the bare alumina support. This points toward low metal–support interaction and hence, a well dispersed catalyst resulting in more available lattice oxygen for ODH. This finding was further confirmed with XRD where the only peaks shown are the ones for the alumina support. This also proves that no vanadium-aluminates are formed due to the interaction between VO_x and the Al_2O_3.

(v) Ethane ODH runs in a fluidized bed CREC Riser Simulator show that in an oxygen-free environment, the prepared catalyst provides promising ethane conversions (6.47–27.64%), ethylene selectivity (57.62–84.51%) and catalyst stability during multiple reduction cycles at 550–600 °C.

(vi) Ethane ODH reaction runs also prove that the absence of gas-phase oxygen is critical for the selective conversion of ethane into ethylene. The prepared catalyst displays a stable performance even after ten repeated ethane pulses. This demonstrates the major role of lattice oxygen in sustaining the ODH over several reaction cycles.

Acknowledgements

The authors wish to thank the National Sciences and Engineering Research Council of Canada (NSERC) for the financial support of this research. The authors would also like to gladly acknowledge the Saudi Arabian Oil Company (Saudi ARAMCO) for the scholarship awarded to Mr. S. Al-Ghamdi during the development of this research, as part of his Ph.D. program at the University of Western Ontario.

References

[1] D. Dharia, W. Letzsch, H. Kim, D. McCue, L. Chapin, Hydrocarb. Process. 83 (4) (2004) 61–66.
[2] R. Anon, Oil Gas J. 102 (8) (2004) 50–52.
[3] M. Bhasin, Top. Catal. 4 (2003) 145–149.
[4] D. Resasco, G. Haller, Catalytic Dehydrogenation of Lower Alkanes, in: Catalysis, vol. 11, Royal Society of Chemistry, 1994.
[5] K.Y.G. Chan, F. Inal, S. Senkan, Ind. Eng. Chem. Res. 37 (3) (1998) 901–907.
[6] T. Ren, M. Patel, K. Blok, Energy 31 (March (4)) (2006) 425–451.
[7] R. Farrauto, C.H. Bartholomew, Fundamentals of Industrial Catalytic Processes, 1st ed., Chapman & Hall, London, 1997.
[8] Z. Shen, J. Liu, H. Xu, Y. Yue, W. Hua, W. Shen, Appl. Catal. A: Gen. 356 (2) (2009) 148–153.
[9] L. Čapek, R. Bulánek, J. Adam, L. Smoláková, H. Sheng-Yang, P. Čičmanec, Catal. Today 141 (3–4) (2009) 282–287.
[10] X. Shi, S. Ji, K. Wang, Catal. Lett. 4 (2008) 331–339.
[11] L. Čapek, J. Adam, T. Grygar, R. Bulánek, L. Vradman, G. Košová-Kučerová, P. Čičmanec, P. Knotek, Appl. Catal. A: Gen. 342 (1–2) (2008) 99–106.
[12] F. Klose, T. Wolff, H. Lorenz, A. Seidelmorgenstern, Y. Suchorski, M. Piorkowska, H. Weiss, J. Catal. 247 (2) (2007) 176–193.
[13] B. Danica, A. Desislava, P. Mirko, H. Stefan, J. Serb. Chem. Soc. 72 (2) (2007) 183–192.
[14] N. Haddad, E. Bordes Richard, L. Hilaire, A. Barama, Catal. Today 2 (2007) 256–263.
[15] G. Karamullaoglu, T. Dogu, Ind. Eng. Chem. Res. 46 (22) (2007) 7079–7086.
[16] B. Tope, Y. Zhu, J.A. Lercher, Catal. Today 4 (2007) 113–121.
[17] F. Cavani, N. Ballarini, A. Cericola, Catal. Today 4 (2007) 113–131.
[18] A.A. Lemonidou, E. Heracleous, Catal. Today 112 (2006) 23–27.
[19] B. Solsona, A. Dejoz, T. Garcia, P. Concepcion, J.M. López-Nieto, M. Vazquez, M.T. Navarro, Catal. Today 3 (2006) 228–233.
[20] E. Heracleous, A.A. Lemonidou, J. Catal. 237 (1) (2006) 175–189.
[21] E. Heracleous, A.A. Lemonidou, J. Catal. 237 (1) (2006) 162–174.
[22] P. Botella, A. Dejoz, J.M. López-Nieto, P. Concepcion, M. Vazquez, Appl. Catal. A: Gen. 298 (2006) 16–23.
[23] K. Nakagawa, T. Miyake, T. Konishi, T. Suzuki, J. Mol. Catal. A: Chem. 260 (1–2) (2006) 144–151.
[24] J.M. López-Nieto, P. Botella, E. García-González, A. Dejoz, M. Vazquez, J. González-Calbet, J. Catal. 225 (2) (2004) 428–438.
[25] E.A. Mamedov, V.C. Corberfin, Appl. Catal. A: Gen. 127 (1995) 1–40.
[26] K. Chen, J. Catal. 195 (October (2)) (2000) 244–252.
[27] H. Kung, Adv. Catal. 40 (1994) 1–38.
[28] K. Chen, A. Khodakov, J. Yang, A.T. Bell, E. Iglesia, J. Catal. 333 (1999) 325–333.
[29] A.T. Bell, A. Khodakov, B. Olthof, E. Iglesia, J. Catal. 181 (1999) 205–216.
[30] K. Chen, S. Xie, A.T. Bell, E. Iglesia, J. Catal. 198 (2) (2001) 232–242.
[31] B. Grzybowska, A. Klisińska, S. Loridant, J. Stoch, I. Gressel, Appl. Catal. A: Gen. 309 (1) (2006) 17–27.
[32] B. Grzybowska, A. Klisińska, K. Samson, I. Gressel, Appl. Catal. A: Gen. 309 (1) (2006) 10–16.
[33] M.V. Martinez-Huerta, X. Gao, H. Tian, I.E. Wachs, J.L.G. Fierro, M.A. Bañares, Catal. Today 4 (2006) 279–287.
[34] R. Grabowski, J. Sloczynski, Chem. Eng. Process. 44 (10) (2005) 1082–1093.
[35] E. Heracleous, M. Machli, A.A. Lemonidou, I.A. Vasalos, J. Mol. Catal. A: Chem. 232 (1–2) (2005) 29–39.
[36] E.P. Reddy, R.S. Varma, J. Catal. 221 (2004) 93–101.
[37] F. Bozon-Verduraz, D.I. Enache, E. Bordes Richard, A. Ensuque, Appl. Catal. A: Gen. 278 (2004) 103–110.
[38] F. Bozon-Verduraz, D.I. Enache, E. Bordes Richard, A. Ensuque, Appl. Catal. A: Gen. 278 (2004) 93–102.
[39] M.T. Navarro, T. Blasco, B. Panzacchi, F. Rey, P. Concepción, J.M. López-Nieto, Catal. Today 96 (2004) 179–186.
[40] Z. Zhao, Y. Yamada, A. Ueda, H. Sakurai, T. Kobayashi, Catal. Today 95 (2004) 163–171.
[41] G. Busca, M. Panizza, C. Resini, F. Raccoli, R. Catani, S. Rossini, Chem. Eng. J. 93 (2003) 181–189.
[42] A.T. Bell, E. Iglesia, M.D. Argyle, K. Chen, J. Phys. Chem. B 106 (2002) 5421–5427.
[43] H.I. DeLasa, M. Volpe, G. Tonetto, Appl. Catal. A: Gen. 272 (1–2) (Sep 2004) 69–78.
[44] A.T. Bell, A. Dinse, R. Schomäcker, Phys. Chem. Chem. Phys. 11 (29) (2009) 6119–6124.
[45] F. Cavani, Catal. Today 24 (1995) 307–313.
[46] M.A. Bañares, Catal. Today 51 (1999) 319–348.
[47] M.A. Bañares, M.V. Martinez-Huerta, X. Gao, I.E. Wachs, J.L.G. Fierro, Catal. Today 61 (2000) 295–301.
[48] I.E. Wachs, B.M. Weckhuysen, Appl. Catal. 157 (1997) 67–90.
[49] B. Wan, C. Kao, K. Huang, Ind. Eng. Chem. Res. 33 (1994) 2066–2072.
[50] M. Volpe, M.L. Ferreira, J. Mol. Catal. A: Chem. 164 (2000) 281–290.
[51] M.L. Ferreira, M. Volpe, J. Mol. Catal. A: Chem. 184 (1–2) (2002) 349–360.
[52] Z. Wu, H. Kim, P.C. Stair, S. Rugmini, S.D. Jackson, J. Phys. Chem. B (2005) 2793–2800.
[53] E. Sham, V. Murgia, J.C. Gottifredi, E.M.F. Torres, Latin Am. Appl. Res. 34 (2004) 75–82.
[54] A.T. Bell, E. Iglesia, M.D. Argyle, K. Chen, J. Catal. 208 (2002) 139–149.
[55] F. Arena, F. Frusteri, A. Parmaliana, Appl. Catal. A: Gen. 176 (1999) 189.
[56] J.M. López-Nieto, T. Blasco, Appl. Catal. A: Gen. 157 (1997) 117–142.
[57] A. Auroux, J. Le Bars, M. Forissier, J.C. Vedrine, J. Catal. 162 (1996) 250–259.
[58] S. Yoshida, T. Tanaka, Y. Nishima, H. Mizutani, 9th International Congress of Catalysis, 1988, p. 1473.
[59] K. Fukudome, N. Ikenaga, T. Miyake, T. Suzuki, Catal. Sci. Technol. (1) (2011) 987–998.
[60] S.M. Al-Zahrani, A.E. Abasaeed, M. Putra, Catal. Commun. 26 (2012) 98–102.
[61] X. Lin, K.R. Poeppelmeier, E. Weitz, Appl. Catal. A: Gen. 381 (1–2) (2012) 114–120.
[62] M. Piumetti, B. Bonelli, P. Massiani, Y. Millot, S. Dzwigaj, L. Gaberova, M. Armandi, E. Garrone, Microporous Mesoporous Mater. 142 (1) (2011) 45–54.
[63] M. Piumettia, B. Bonell, P. Massiani, S. Dzwigaj, I. Rossetti, S. Casale, M. Armandi, C. Thomas, E. Garrone, Catal. Today 179 (1) (2012) 140–148.
[64] O. Rubio, J. Herguido, M. Menendez, Chem. Eng. Sci. 58 (2003) 4619–4627.
[65] J. Soler, J.M. López-Nieto, J. Herguido, M. Menendez, J. Santamaria, Ind. Eng. Chem. Res. 38 (1999) 90–97.
[66] O. Rubio, J. Herguido, M. Menendez, AIChE J. 50 (7) (2004) 1510–1522.
[67] A.A. Lemonidou, Appl. Catal. A: Gen. 216 (2001) 277–284.
[68] M.D. Argyle, Oxidative Dehydrogenation of Light Alkanes on Metal Oxide Catalysts, University of California, Berkeley, 2003.
[69] T. Blasco, A. Galli, J.M. López-Nieto, F. Trifiro, J. Catal. 169 (1997) 203–211.

[70] J.L.G. Fierro, J.M. López-Nieto, G. Kremenic, Appl. Catal. 61 (1990) 235–251.
[71] A. Gervasini, P. Carniti, J. Keränen, L. Niinistö, A. Auroux, Catal. Today 96 (2004) 187–194.
[72] I.E. Wachs, Y. Chen, J. Jehng, L.E. Briand, T. Tanaka, Catal. Today 78 (2003) 13–24.
[73] N. Ballarini, F. Cavani, A. Cericola, C. Cortelli, M. Ferrari, G. Capannelli, A. Comite, R. Catani, U. Cornaro, Catal. Today 92 (2004) 99–104.
[74] H.I. DeLasa, Canadian Patent 1,284,017 (1991); USA Patent 5,102,628 (1992).
[75] A. Auroux, Top. Catal. 4 (1) (1997) 71–89.
[76] H. Miyata, K. Fujii, T. Ono, J. Chem. Soc., Faraday Trans. 1 84 (9) (1988) 3121–3128.
[77] J. Datka, A.M. Turek, M. Jheng, I.E. Wachs, J. Catal. 135 (1992) 186–199.
[78] R.J. Cvetanović, Y. Amenomiya, Adv. Catal. 17 (1967) 103–149.
[79] G. Tonetto, J. Atias, H.I. DeLasa, Appl. Catal. A: Gen. 270 (1–2) (2004) 9–25.
[80] R. Farrauto, C.H. Bartholomew, Fundamentals of Industrial Catalytic Processes, Chapman & Hall, London, UK, 1997.
[81] M.G. White, Heterogeneous Catalysis, Printice Hall, Inc., Upper Saddle River, NJ, USA, 1999.
[82] K.E. Sedor, M.M. Hossain, H.I. DeLasa, Chem. Eng. Sci. 63 (2008) 2994–3007.
[83] M.A. Alvarez-Merino, J.P. Joly, F. Carrasco-Marín, C. Moreno-Castilla, J. Colloid Interface Sci. 260 (2003) 449–453.
[84] S.A. Al-Ghamdi, M. Volpe, H.I. DeLasa, 22nd NAM Catalysis Conference, Detroit, 2011.